# 20-fs Pulse Shaping With a 512-Element Phase-Only Liquid Crystal Modulator

H. Wang, *Student Member, IEEE*, Z. Zheng, *Member, IEEE*, D. E. Leaird, *Member, IEEE*, A. M. Weiner, *Fellow, IEEE*, T. A. Dorschner, *Associate Member, IEEE*, J. J. Fijol, L. J. Friedman, *Member, IEEE*, H. Q. Nguyen, and L. A. Palmaccio

***Abstract*—We report pulse shaping experiments in the 20-fs range using a 512-element phase-only liquid crystal modulator array. The results demonstrate the potential for significantly improved spectral resolution compared to 128-element liquid crystal modulators previously used for pulse shaping. Furthermore, we show that subtle nonlinear spatial dispersion has a profound effect on replica pulses arising due to the pixellated nature of a liquid crystal modulator and may dramatically reduce their (already low) peak intensity.**

***Index Terms*—Liquid crystal devices, optical pulse shaping.**

## I. Introduction

PULSE SHAPING techniques using programmable spatial light modulators (SLMs) have become a powerful tool for ultrafast scientific studies as well as in applications such as optical communications [1], [2]. The performance parameters of the optical modulator, including the space-bandwidth product, speed, and insertion loss, can have a significant impact on the capability of the pulse shaper. Furthermore, there is now increasing activity in applying pulse shaping to pulses in the few tens of femtoseconds range and below. For now, the most popular SLMs for programmable pulse shaping are liquid crystal modulators (LCMs) [3], [4], acoustooptic (AO) modulators [5], and deformable mirrors [6], [7]. AO devices have offered the highest space-bandwidth products, but their diffraction efficiency [5] is generally low and they are only generally applicable with amplified (not high repetition rate) systems. Furthermore, their use has not yet been demonstrated in the sub-50 fs regime. Deformable mirrors have been used successfully to trim out small amounts of dispersion in the sub-20 fs range [7] and also for selective enhancement of high harmonic generation [8], but their applications are limited by their relatively small effective pixel count. LCMs are currently the most widely used SLMs in femtosecond pulse shapers. Their use for shaping of sub-15 fs pulses has already been demonstrated [9]–[11]. However, previous devices were limited to 128 pixels, which puts constraints on the spectral resolution and the temporal window that could be realized by the pulse shapers. Here we report experiments, performed in the 20-fs regime, which for the first time demonstrate pulse shaping using a 512-element phase-only LCM. A preliminary report of this work was given in [12] after the period. The number of features that can be programmed onto the spectrum in our experiments is now comparable to that reported in pulse shaping using AO modulators. Our results show the potential of using such devices for high-accuracy pulse shaping with significantly improved spectral resolution and temporal window.

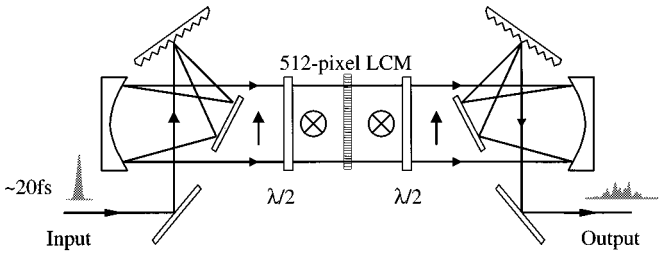


Fig. 1. Layout of the pulse shaper.

In addition to basic pulse-shaping studies, we also characterized the low-intensity replica pulses [3], which are known to occur due to the pixellated nature of an LCM pulse shaper. Our investigation shows that a subtle nonlinear spatial dispersion has a profound effect on the character of the replica pulses and may dramatically reduce their (already low) peak intensity. This modification of the form of the replica pulses, which has not previously been reported, is especially significant due to the wide optical bandwidth and the large number of LCM pixels.

The remainder of this paper is structured as follows. The experimental setup is discussed in Section II. Section III shows the results of some typical pulse-shaping experiments. The phenomena of temporal window and replica pulses in our pulse-shaping experiments are studied in Section IV. Section V is the conclusion.

## II. Experimental Setup

As shown in Fig. 1, in our pulse shaper, we used two 600-grooves/mm diffraction gratings and two 300-mm radius spherical mirrors. Two zero-order half-wave plates are used to adjust the state of polarization between the gratings and the LCM. The incident angle onto the grating was approximately 28°, and the diffracted beam at the center wavelength was nearly normal to the grating surface.

Manuscript received January 8, 2001. This work was supported in part by the National Science Foundation under Grants 9900369-ECS and 9722668-PHY.

H. Wang, D. E. Leaird, and A. M. Weiner are with the School of Electrical and Computer Engineering, Purdue University, West Lafayette, IN 47907-1285 USA (e-mail: wangh@ecn.purdue.edu).

Z. Zheng was with the School of Electrical and Computer Engineering, Purdue University, West Lafayette, IN 47907-1285 USA and now he is with Lucent Technologies, Holmdel, NJ 07733 USA.

T. A. Dorschner, J. J. Fijol, L. J. Friedman, H. Q. Nguyen, and L. A. Palmaccio are with Raytheon Company, Lexington, MA 02421 USA (e-mail: Terry_A_Dorschner@res.raytheon.com).

Publisher Item Identifier S 1077-260X(01)09943-9.

1077–260X/01$10.00 © 2001 IEEE

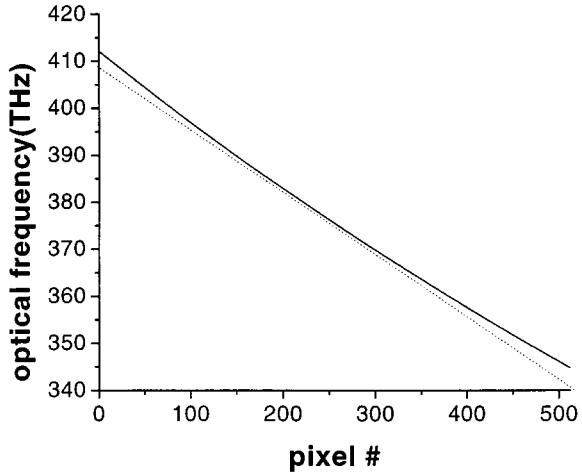


Fig. 2. Optical frequency versus pixel# relationship. Solid curve: measured results. Dotted line: linear approximation.

The LCM is based on an advanced liquid crystal modulator array technology that was previously developed for beam steering in laser radar applications [13]. We used a phase-only modulator array with 512 modulator elements. E46 liquid crystal was used in this modulator, and the molecules were aligned parallel to the electrodes. The center-to-center spacing of adjacent pixels was 25 $\mu$m for a total spatial aperture of 12.8 mm. The LCM was controlled by a custom interface card in a laboratory computer, which could be programmed using Matlab or C++. The reprogramming time of the LCM was about 90 ms, which we will demonstrate later.

In our pulse-shaper setup, the average frequency difference $\Delta f$ between adjacent pixels was 130 GHz, and the pixels of the LCM covered the spectrum from 722.5 to 872.5 nm. The input beam diameter was 6 mm, and the calculated diffraction limit for the diameter of the focused beam at the mask plane was 22 $\mu$m, which was less than the size of a single LCM pixel. This is a necessary condition in order to effectively utilize the full number of LCM pixels.

Our experiments used $\sim$20 fs pulses generated from a mode-locked Ti : sapphire laser from KML Labs. The full-width at half-maximum (FWHM) of the laser spectrum was 60 nm. The laser spectrum was cut off by the LCM aperture at 722.5 and 872.5 nm. The power at 722.5 nm was 3.6% of the peak value, and that at 872.5 nm was 3.0% of the peak value. Shaped pulses were measured by intensity cross-correlation using unshaped pulses split off from the laser as a reference. Because of the large bandwidth, the mapping between the linearly spaced pixels on the LCM and the actual optical frequency was not strictly linear [14]. To obtain high-quality pulse-shaping results while making use of the increased pixel count in our LCM array, it was essential to take into account and compensate this effect. This was achieved by using a detailed mapping procedure to correctly calibrate the pixel number versus optical frequency relationship, which was then used in programming the LCM [14]. The mapping is shown in Fig. 2. The solid curve is the measured data and the dotted line is the linear fit. The importance of this nonlinear mapping will be demonstrated later. Because of the large bandwidth, it was also important to store different phase versus voltage calibration curves for different pixels corresponding to different wavelengths, since the phase versus voltage relationship changes with frequency. To this end, we calibrated the device at four wavelengths (543, 633, 850, and 1064 nm). We then calculated the calibration curves at other wavelengths using an equation for the birefringence versus wavelength dependence of the E46 liquid crystal

$$\Delta n(\lambda) = g\lambda^2\lambda_{st}^2/(\lambda^2 - \lambda_{st}^2) \tag{1}$$

where $g = 2.920 \times 10^{-6}$ nm$^{-2}$ and $\lambda_{st} = 257.4$ nm were obtained by fitting (1) to the calibration data. This equation was acquired based on a phenomenological theory applied by Wu [15]. The distance between the gratings in the pulse shaper was adjusted so that when there was no voltage on the LCM, the cross-correlation trace had the same width as the autocorrelation trace of the input laser pulse. The above calibration procedure ensured the accuracy of the spectral phase function we added onto the LCM in the experiments.

## III. Pulse-Shaping Experimental Results

We present a number of pulse-shaping results with either binary or gray-level phase modulations applied to the LCM. When applying a binary function to the LCM, each pixel is set for either 0 phase (symbol "0") or $\pi$ phase (symbol "1"). The set of phases applied to the LCM pixels was determined by sampling the desired frequency-domain phase function at the optical frequencies corresponding to the center positions of the individual pixels, using the measured pixel number versus optical frequency mapping.

In Fig. 3(a) and (b), we applied a linear spectral phase modulation with a total phase shift of $256\pi$ across the array (average of $\pi/2$ phase shift per pixel) to shift the pulse in the time domain by $1/4\Delta f$ ($\sim$1.9 ps) according to the relation

$$\tau = -\frac{\partial\psi(\omega)}{\partial\omega} \tag{2}$$

where $\psi(\omega)$ is the spectral phase. In Fig. 3(a), the nonlinear mapping of frequency versus pixel # (Fig. 2) was used to generate the phase array, which results in a clean shift of the pulse away from zero delay without distortion, as desired. In Fig. 3(b), a linear mapping was used. As a result, the phase function was linear with respect to pixel#. Due to the nonlinear frequency versus pixel# relationship, the slope of the actual spectral phase function varies within the spectrum, leading to $\sim$15% different delays for different parts of the spectrum. This results in a distorted pulse broadened substantially to $\sim$300 fs, with a corresponding reduction in peak intensity (notice different intensity scales in the plots). These data clearly demonstrate the importance of accounting for the nonlinear spectral dispersion.

As another example, in Fig. 3(c) and (d) we applied a periodic 0–$\pi$–0–$\pi$ spectral phase modulation, with two LCM pixels per symbol on the average. This is expected to split the input pulse into a pair of pulses displaced by $\pm 1/4\Delta f$ about the time origin, with the same pulse durations as the input. This is indeed observed in Fig. 3(c), where the measured nonlinear spectral

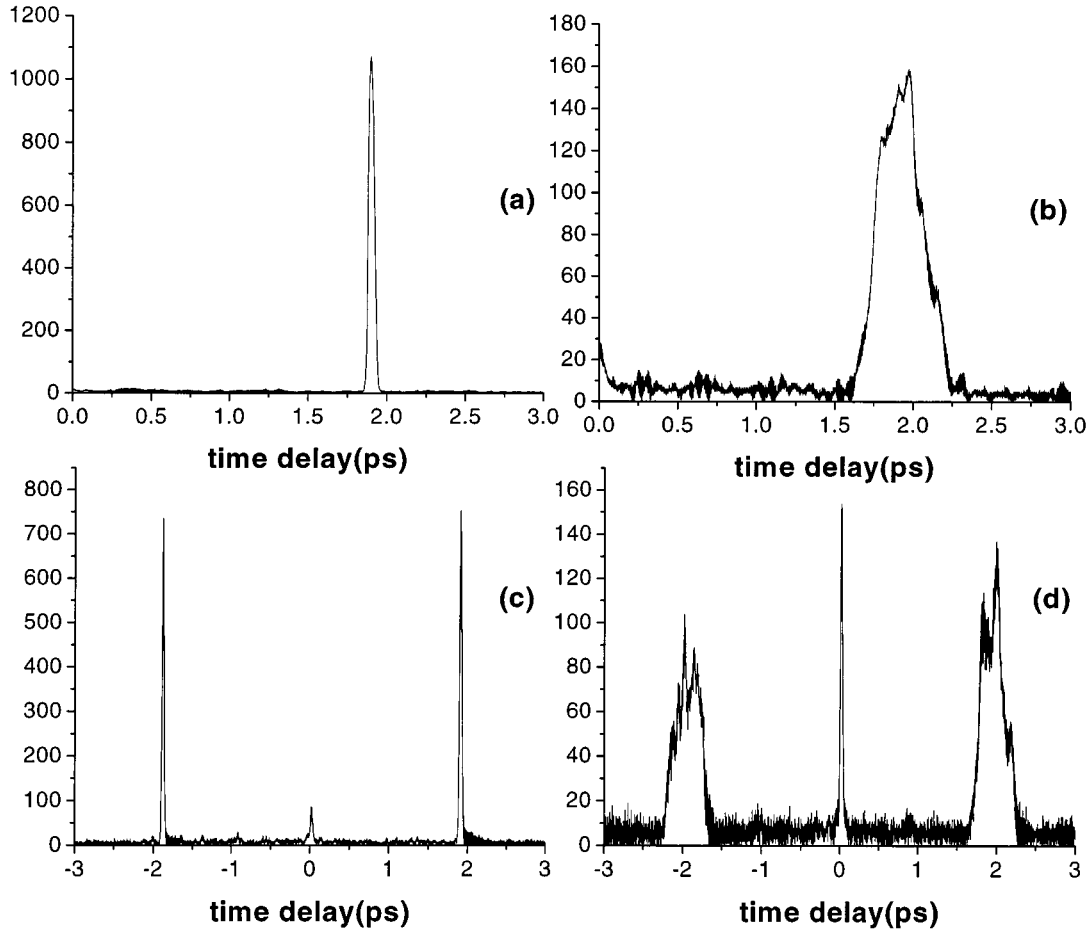


Fig. 3. (a) Cross-correlation trace of linear phase modulation (total $256\pi$ phase shift over LCM), using the nonlinear mapping of optical frequency versus pixel#. (b) The same modulation as in (a), but assuming a linear mapping. (c) Cross-correlation traces of periodic $0$–$\pi$–$0$–$\pi$ modulation when the spectrum was divided into 256 bins (i.e., $00\pi\pi00\pi\pi$, etc.), using the nonlinear mapping. (d) The same modulation as in (b), but assuming a linear mapping.

dispersion curve was used. In Fig. 3(d), however, where a linear spectral dispersion was assumed, the results are very different. The input pulse is still split into a doublet, with about the same time delays as in Fig. 3(c). But both pulses are distorted and broadened to $\sim$300 fs. The reason is similar to that discussed for Fig. 3(a) and (b). Although the spectral phase varies from zero to $\pi$ every two pixels exactly, the frequency span corresponding to two pixels varies throughout the spectrum, once again leading to different delays for different parts of the spectrum. We note that the feature observed at $t = 0$ may be attributed to a slight amplitude error in applying the $\pi$ phase. This peak becomes more pronounced in Fig. 3(d) due to the reduced intensity of the main pulses at $\pm$1.9 ps.

Fig. 4 shows the results of periodic $0$–$\pi$–$0$–$\pi$ spectral phase modulations. In Fig. 4(a), each "bit" ($0$ or $\pi$) corresponds to four pixels on the average, while in Fig. 4(b) every "bit" covered two pixels and in Fig. 4(c) one pixel on the average. In all of these data, the measured frequency versus pixel number curve was used. As in Fig. 3, two pulses were generated under this kind of modulation. They were distributed symmetrically about zero delay, and the distance between them was inversely proportional to the period of modulation function. Thus in Fig. 4(a), the LCM works like a 128-pixel LCM. In comparison, in Fig. 4(c), where the full capability of the 512-element LCM is utilized, the output pulses are spread by a factor of four more. This illustrates a key benefit of the four-fold increase in pixel count: pulse shaping can access a four times larger time window for a fixed optical bandwidth.

Fig. 5 shows the results when we used periodic M-sequence phase modulations. M-sequences are pseudonoise digital sequences that are useful in communications [16]. The length-7 M-sequence we used is (0 0 1 0 1 1 1); the length-15 M-sequence is (0 0 0 1 0 0 1 1 0 1 0 1 1 1 1). In programming the LCM, we applied 0 phase for an M-sequence value of zero and $\pi$ phase for an M-sequence value of one. Previous work has shown that applying a periodic repetition of an M-sequence to the spectral phase leads to a train of femtosecond pulses under a smooth envelope, with the number of pulses in the train roughly equal to the length of the M-sequence code and with the central pulse suppressed [1], [17]. We can see several such pulse trains in Fig. 5. In Fig. 5(a) and (d), one LCM pixel is assigned to each M-sequence bit. In Fig. 5(b) and (e) and in Fig. 5(c) and (f), two and four LCM pixels are assigned to each M-sequence bit, respectively, which means that these cases emulate 256-pixel and 128-pixel LCMs, respectively. As we can see, when the number of pixels per M-sequence bit increases, the intervals between the pulses become smaller, and also the time window becomes narrower. Therefore, the results using all 512 pixels [Fig. 5(a) and (d)] show an improved time window compared to the case where only 128 independent pixels are used [Fig. 5(c)

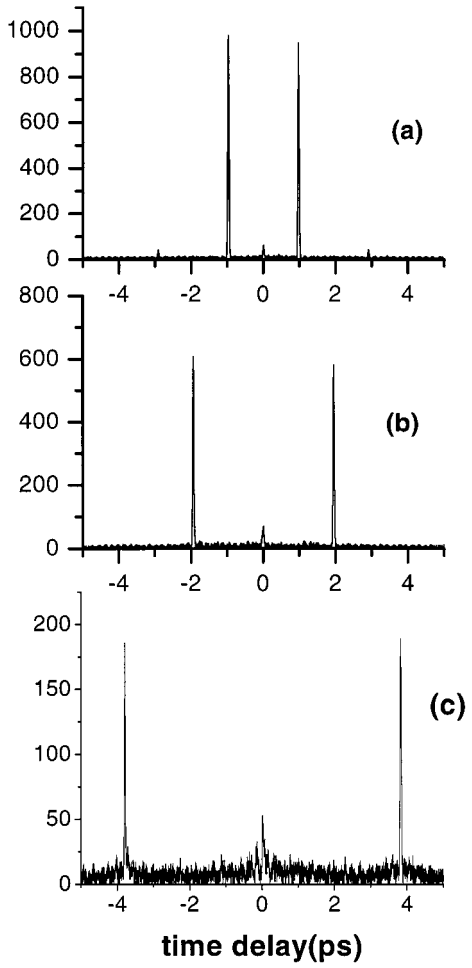


Fig. 4. Periodic 0–$\pi$–0–$\pi$ modulation: (a) four pixels per digit, total 128 bins, (b) two pixels per digit, total 256 bins, and (c) one pixel per digit, total 512 bins.

and (f)]. However, the rolloff in Fig. 5(a) and (d) appeared to be somewhat faster than we expected, which we will discuss in a later section.

We also report some preliminary work on adaptive pulse shaping [10]. Because our LCM electronics are faster than the commercial LCM electronics used in [10] and other works (where a 500 ms update time was quoted), this can potentially speed the time to convergence for an adaptive pulse-shaping system. In our work, we first distorted the pulse by moving one of the pulse-shaper diffraction gratings away from the zero-dispersion point. The cross-correlation trace was broadened to give a width of 122 fs FWHM. We used the second harmonic (SH) power from a KDP crystal as the figure of merit of the shaped pulse. The computer that controlled the LCM detected the SH signal as a feedback parameter and adaptively adjusted the voltage array on the LCM to achieve the best SH power.

To keep the loop time fast, we used a very simple algorithm. The 512 pixels of the LCM were divided into 16 sections, each consisting of 32 pixels. The voltage array was assumed linear within each section. That was, we used 16 sections of lines to form an approximate curve. There were a total of 17 independent parameters. These were randomly changed each iteration, and only changes that improved the figure of merit (average SH power) were kept. The amount of the change introduced was weighted to be smaller in the stronger parts of the spectrum and decreased with iteration number. The random change of parameter $j$ at iteration $i$ is

$$\Delta V(i, j) = r(i, j)S(j)(1 - i/N) \tag{3}$$

where $r(i, j)$ is the random number within a certain range, $S(j)$ is the factor related to the spectral power at the point of parameter $j$, and $N$ is the predetermined total number of iterations. As we can see in Fig. 6, the distorted pulse was almost restored by the adaptive pulse-shaping program. The resulting cross-correlation trace is 31 fs FWHM, which corresponds to a roughly 20 fs pulse after deconvolving the 20 fs duration of the reference pulse.

In our experiments, it took about 120 ms to run a single iteration. Of this time, 90 ms is used to update the drive levels of the LCM. This time is limited mainly by the settling time of the liquid crystal molecules themselves; the drive electronics are appreciably faster than this. This is in contrast to most current LCM drive electronics, which limit the update time to $\sim$500 ms [10]. Fig. 7 shows the average SH power versus time, when we switched the voltage array on the LCM back and forth between a flat phase case and a prespecified random voltage array. It shows that 80$\sim$90 ms is enough to update the drive levels of the LCM. The system can run at this speed indefinitely while changing to new randomly selected LCM settings at each iteration. Recently, for a thermally controlled transmissive device operating at 1064 nm, Raytheon Company has measured an LCM switching time of approximately 10 ms. A comparable device designed for 850 nm should operate at a switching time of $10^{*}(850/1064)^2 = 6.4$ ms [the $(850/1064)^2$ factor would arise from the decreased thickness needed for the 850-nm wavelength].

## IV. Study of Temporal Window and Replica Pulse Effects

In pulse-shaping experiments, the intensity of the output waveform will be modulated by a temporal window function [1]. Outside a certain temporal range, the pulse will be too weak to be useful. There are two factors that determine the temporal window. One is the finite size of the individual focused frequency components, which affects any pulse shaper. The second is the pixel structure of the LCM, which applies only to pixellated SLMs. In the following, we briefly review these temporal window effects and then characterize them experimentally for our system. We will also see that the nonlinear frequency versus pixel number relation, which is described here for the first time, plays an important role in the effects related to the discrete pixels.

Assuming the input laser beam has a Gaussian spatial profile, any individual optical frequency component focused onto the LCM plane also has a spot with a Gaussian profile. From [1] and [18], the field immediately after the LCM can be written as

$$E_m(x, \omega) \sim E_{in}(\omega)e^{-(x-\alpha\omega)^2/w_0^2}M(x). \tag{4}$$

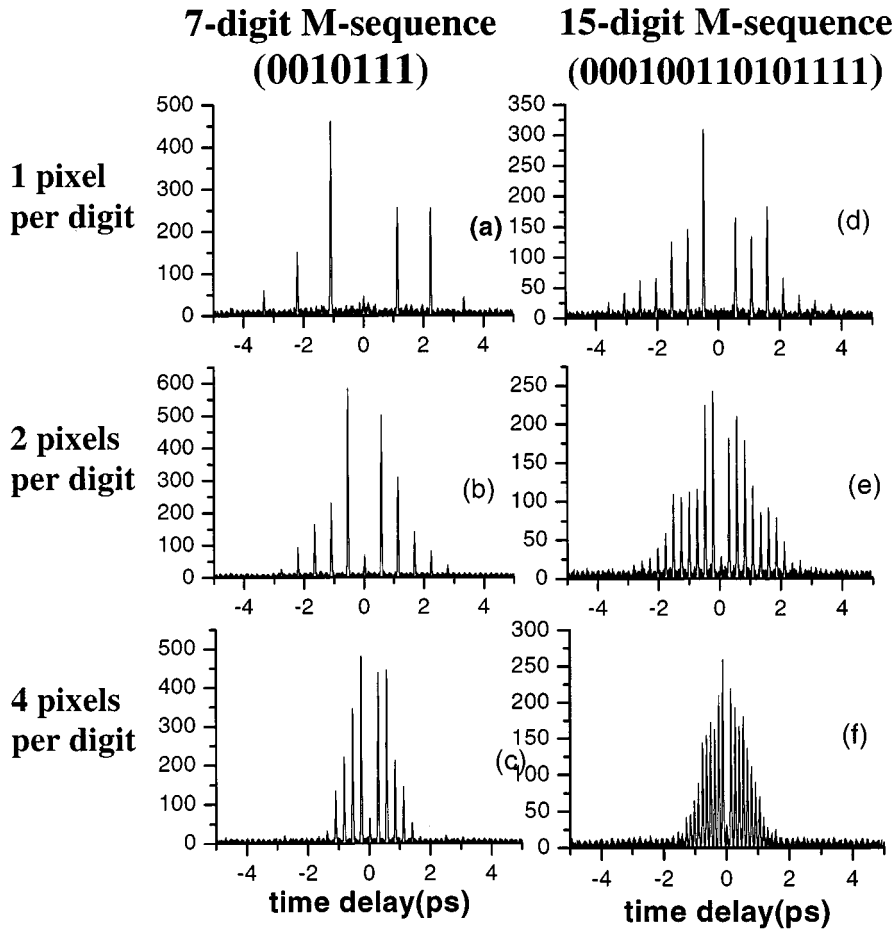


Fig. 5. Periodic M-sequence modulation: (a)–(c) 7-digit M-sequence, (d)–(f) 15-digit M-sequence. (a), (d) Total 512 bins; (b), (e) total 256 bins; (c), (f) total 128 bins.

where $M(x)$ is the mask function and $x$ is the direction perpendicular to the boundaries of the pixels. $w_0$ is the focused Gaussian beam radius at the focal plane of the spherical mirrors (assuming diffraction-limited focusing); $\alpha$ represents the spatial dispersion at the LCM plane. $\alpha$ and $w_0$ are

$$\alpha = \frac{\partial x}{\partial \omega} = \frac{\lambda^2 F}{2\pi c d \cos\theta_d} \tag{5}$$

$$w_0 = \frac{\cos\theta_{in}}{\cos\theta_d}\left(\frac{F\lambda}{\pi w_{in}}\right). \tag{6}$$

Here $w_{in}$ is the beam radius of the input beam; $\theta_{in}$ and $\theta_d$ are the incident angle and diffraction angle on the grating; $F$ is the focal length of the spherical mirror; and $\lambda$ is the center frequency of the laser spectrum.

Equation (4) is a nonseparable function of both space $x$ and frequency $\omega$. To obtain an output field that is a function of frequency only, one must perform an appropriate spatial filtering operation. This was analyzed in [18] by expanding the masked field into Hermite–Gaussian modes and assuming that all of the spatial modes except for the fundamental Gaussian mode are eliminated by the spatial filtering. Such spatial filtering can be accomplished experimentally by passing the output from the pulse shaper through either a single-mode fiber or a regenerative amplifier. Our treatment is also approximately valid when the spatial filtering is performed simply by placing an iris after the pulse-shaping setup. At last, one can derive the filter function of the pulse shaper as

$$H(\omega) = \left(\frac{2}{\pi w_0^2}\right)^{1/2} \int dx M(x) \exp[-2(x-\alpha\omega)^2/w_0^2]. \tag{7}$$

From the Fourier transformation of (7), we can derive the impulse response of the pulse shaper as $h_{\text{eff}}(t) = m(t)g(t)$, where

$$m(t) = \frac{1}{2\pi}\int d\omega M(\alpha\omega) e^{i\omega t} \tag{8}$$

$$g(t) = \exp(-w_0^2 t^2/8\alpha^2). \tag{9}$$

$m(t)$ is the infinite-resolution impulse response and $g(t)$ is an envelope function restricting the temporal window. We see that the temporal window caused by a finite input Gaussian beam also has a Gaussian shape. The FWHM of this temporal window in terms of intensity is

$$T = \frac{4\alpha\sqrt{\ln 2}}{w_0}. \tag{10}$$

For our setup, $T \approx 8.8$ ps.

The temporal window caused by pixellation should be included in $m(t)$. For simplicity, we assume that the pixels are

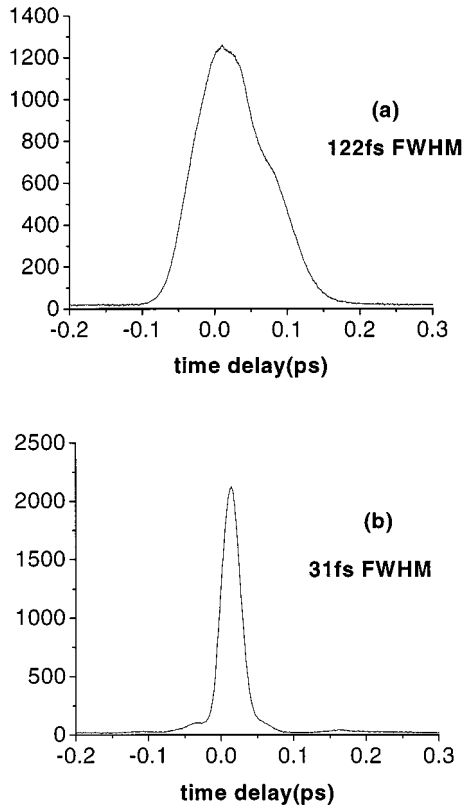


Fig. 6. (a) Cross-correlation trace of the distorted pulse, 122-fs cross-correlation FWHM. (b) Cross-correlation trace of the restored pulse after 10 min, 31-fs cross-correlation FWHM.

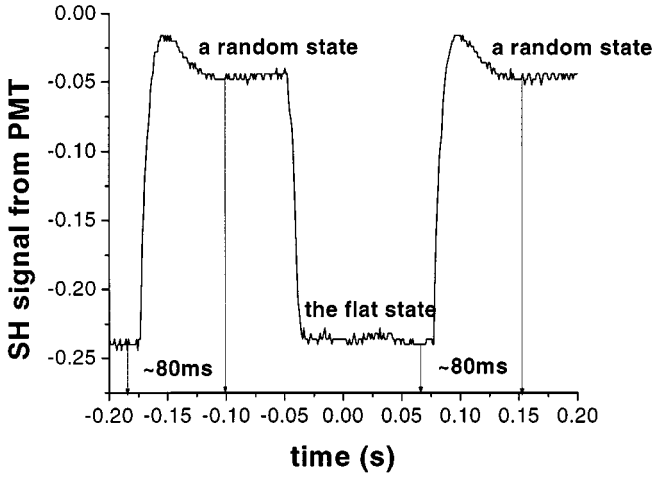


Fig. 7. SH signal versus time, when the LCM was switching between flat phase state and a random state.

distributed linearly versus optical frequency and omit interpixel gaps; then $M(x)$ can be written as [3]

$$M(x) = \left\{ H\left(\frac{x}{\alpha}\right) \sum_n \delta(x - n\Delta x) \right\} * rect\left(\frac{x}{\Delta x}\right) \quad (11)$$

$$M(\alpha\omega) = \left\{ H(\omega) \sum_n \delta(\omega - 2\pi n \Delta f) \right\} * \mathrm{rect}\left(\frac{\omega}{2\pi\Delta f}\right). \quad (12)$$

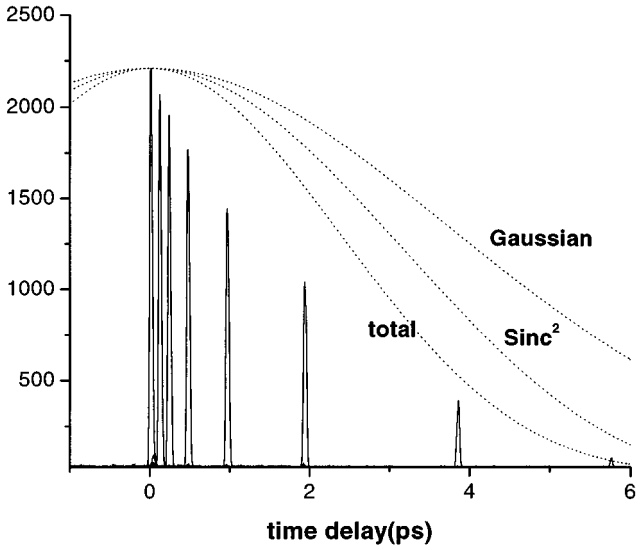


Fig. 8. Temporally shifted pulses using linear phase modulation. From the left-most pulse to the right-most pulse, the total phase increase over the LCM was 0, $16\pi$, $32\pi$, $64\pi$, $128\pi$, $256\pi$, $512\pi$, and $768\pi$, respectively. The dotted curves are theoretical Gaussian window, theoretical Sinc window, and total temporal window (the product of the previous two windows).

Here $H(\omega)$ is the desired filter function, rect$(u)$ is a rectangular function of unit amplitude and width, $*$ denotes convolution, and the summation runs over all LCM pixels. We take $H(\omega)$ to include the truncation of the spectrum outside the region of LCM pixels (outside the region 722.5 to 872.5 nm in our experiments). $\Delta f$ denotes the optical frequency span per pixel. Since $m(t)$ is the inverse Fourier transform of $M(\alpha\omega)$, we have

$$m(t) = \left[ \sum_n h(t - n\Delta f^{-1}) \right] \bullet \mathrm{sinc}\,(\pi \Delta \mathrm{ft}) \quad (13)$$

and therefore

$$h_{\mathrm{eff}}(t) = \left[ \sum_n h(t - n\Delta f^{-1}) \right] \bullet \mathrm{sinc}\,(\pi \Delta \mathrm{ft}) \mathrm{g(t)}. \quad (14)$$

Here $h(t)$ is the desired impulse response function, which would be obtained if the modulation was continuous and $\mathrm{sinc}(t) = \sin t/t$. In our experiments, $\Delta f(\mathrm{average}) = 130$ GHz. We can see, in terms of intensity, the $\mathrm{sinc}^2(\pi \Delta f t)$ term is the contribution to the temporal window function caused by pixellation. The total temporal window function should be the product of the $\mathrm{sinc}^2$ window caused by pixellation and the Gaussian window caused by the finite spot size at the masking plane.

Equation (14) also shows that there is a series of replica impulse response functions $h(t - n\Delta f^{-1})$. The entire result is weighted by the temporal window function. The interval between the nearest replica pulse and the main pulse is $\Delta f^{-1}$, which should be 7.7 ps in our experiments.

Fig. 8 shows experimental results on the temporal window. We applied a series of linear spectral phase modulations to shift the pulse to various positions later in time. Fig. 8 shows intensity cross-correlation traces of the shifted pulse in the time interval $-1$ to 6 ps. The total phase increase across the 512 LCM pixels, from the left-most pulse to the right-most pulse, is 0 (no shift), $16\pi$, $32\pi$, $64\pi$, $128\pi$, $256\pi$, $512\pi$, and $768\pi$, respectively, corresponding to phase shifts of 0, $\pi/32$, $\pi/16$, $\pi/8$, $\pi/4$, $\pi/2$, $\pi$,

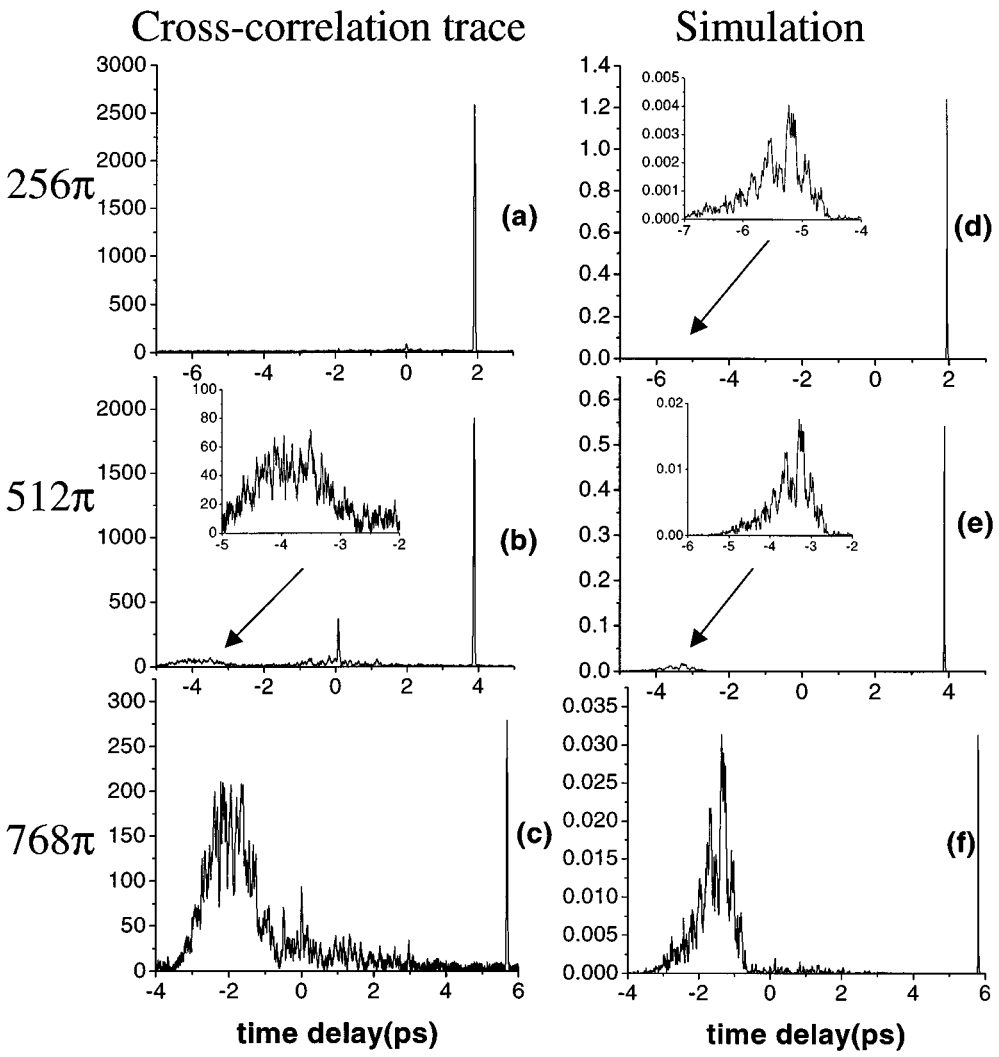


Fig. 9. Linear phase modulation and replica pulses. Total phase increase: (a), (d) $256\pi$; (b), (e) $512\pi$; (c), (f) $768\pi$. (a)–(c) Experimental data; (d)–(f) simulation results.

and $3\pi/2$ per pixel. The observed temporal shifts were consistent with (2), and the shifted pulses exhibit no obvious distortion. The three dotted curves are the theoretical Gaussian temporal window, $\text{Sinc}^2$ temporal window, and estimated total temporal window (the product of the previous two windows). From this figure, we can see that the rolloff of the pulse intensities is described reasonably well by the temporal window predicted by theory. Looking more closely, the initial rolloff is somewhat faster than the prediction, which could be a sign that the actual spectral resolution achieved in our experiments is slightly coarser than the theoretical limits based on diffraction-limited focusing.

We note that each shifted pulse in Fig. 8 should have a replica pulse in the time interval $-8$ ps $< t < 0$ (not shown in the figures). For the case of a truly linear spectral dispersion, the replica amplitudes increase with increasing total phase shift. For a $512\pi$ total phase shift, the replica pulse at $-3.9$ ps would be expected to have the same amplitude as the desired shifted pulse at $+3.9$ ps; while for $768\pi$ total phase shift, the replica pulse at $-1.9$ ps would be expected to be substantially stronger than the desired shifted pulse at 5.8 ps.

The generation of replica pulses can be viewed in the following way. We consider a linear spectral phase function in the frequency domain and assume the pixels are distributed linearly versus frequency. For a phase increase of $\Delta\phi$ per pixel, the pulse should be shifted by $\Delta t_1 = \Delta\phi/2\pi\Delta f$. But equivalently, we can say that the phase shift is increasing by $\Delta\phi - 2\pi$ per pixel (decreasing by $2\pi - \Delta\phi$ per pixel), for which the time shift is $\Delta t_2 = (\Delta\phi - 2\pi)/2\pi\Delta f$. If the phase function we add is continuous in the frequency domain, then of course there can be only one phase slope. But because of the pixellated structure of the LCM, a linear modulation of a positive slope can also be considered a linear modulation of a corresponding negative slope. For this example, it means that while $\Delta t_1$ is a possible point for the different frequency components to form a pulse, $\Delta t_2 = \Delta t_1 - \Delta f^{-1}$ is also a possible point. We can see that the generation of replica pulses is a direct result of the LCM's pixel structure.

However, in our experiments, the generation of replica pulses behaves differently, because the pixels are not distributed linearly versus frequency and $\Delta f$ is no longer constant. Because of this variation of $\Delta f$, different parts of the spectrum give con-

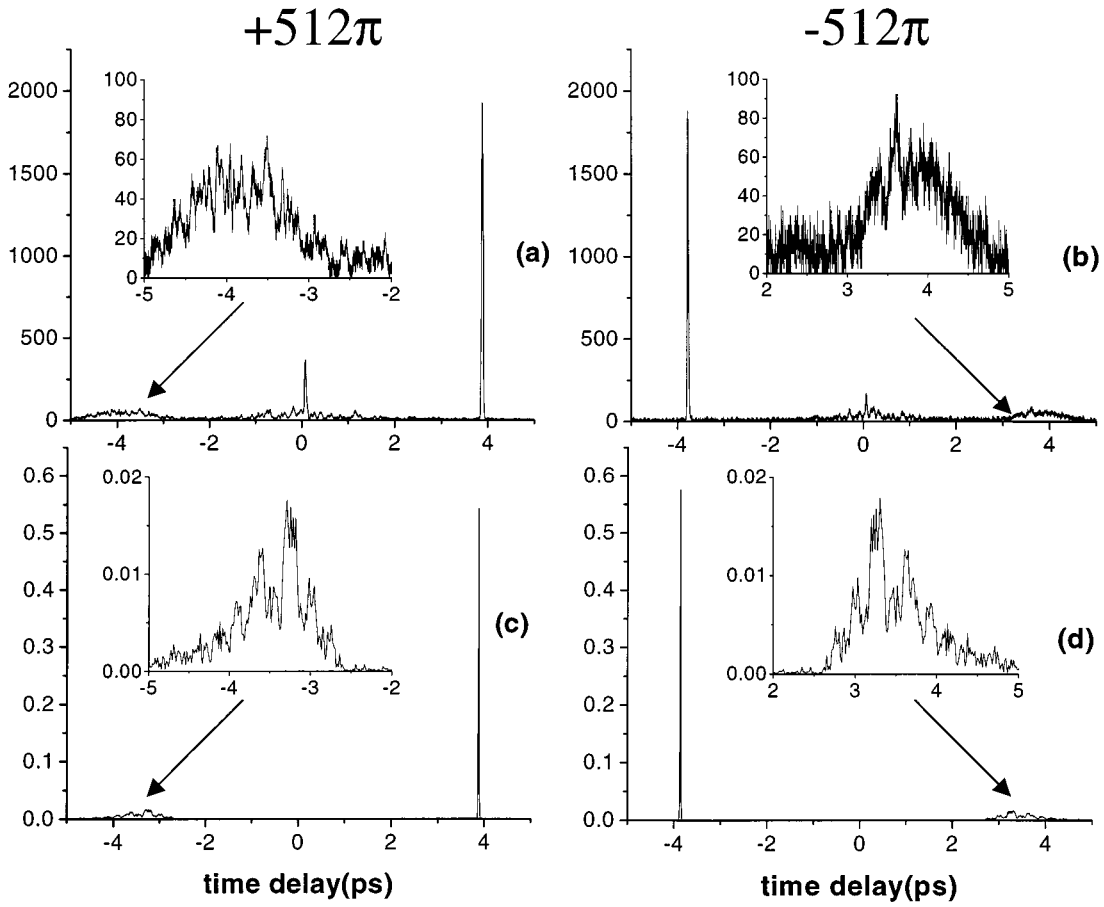


Fig. 10. Linear phase modulation results and replica pulses. (a), (b) Experimental cross-correlation traces; (c), (d) simulation, using the mapping of frequency versus pixel# in Fig. 2. Total phase increase over the LCM: (a), (c) $+512\pi$; (b), (d) $-512\pi$.

tribution to the replica at different time shift, causing the replica to be broadened and chirped, with reduced intensity.

Fig. 9 shows the experimental and simulation results for replica pulses corresponding to the linear spectral phase modulations of $256\pi$, $512\pi$, and $768\pi$ from Fig. 8. We see from Fig. 9 that when the total phase increase was $256\pi$ (pulse shift 2 ps), there was a very weak and chirped replica pulse at around $-6$ ps in the simulation, which was concealed by noise in the experimental data. When the total phase increase was $512\pi$ (pulse shift 4 ps), a chirped replica pulse at about $-4$ ps began to be visible in both simulation and experiment. When the total phase increase was $768\pi$ (pulse shift 6 ps), the replica pulse was at $-2$ ps (closer to zero delay than the main pulse) and its intensity became comparable to that of the main pulse. In all three cases, however, the intensities of the replica pulses are much less than they would be in the case of a linear spectral dispersion.

Another example is shown in Fig. 10. Here we consider a linear spectral phase shift varying by either $+512\pi$ or $-512\pi$ across the 512-pixel array. Ideally, the linear spectral phase shift leads to a pulse temporally shifted by 3.8 or $-3.8$ ps, respectively. However, because the phase shift per pixel is $\pi(-\pi)$, the linear phase function is not adequately sampled by the pixellated array. In fact, in the case of linear spectral dispersion, the intensity of the shaped pulse and the strongest replica pulse should be identical, leading to an equal-intensity pulse pair symmetrically displaced around zero delay. The nonlinear spectral resolution breaks the symmetry. Hence in the case of $+512\pi$ phase shift [Fig. 10(a)], the desired shifted pulse at 3.9 ps retains its 20-fs pulse duration, but the replica at $-3.9$ ps is broadened to 1 ps, with its peak intensity suppressed by a factor of 30. Conversely, for $-512\pi$ spectral phase shift [Fig. 10(b)], the desired pulse at $-3.9$ ps is undistorted, while the replica pulse at $+3.9$ ps is broadened and suppressed. Similar results are obtained from simulation using the actual nonlinear spectral dispersion function [Fig. 10(c) and (d)]. It is also interesting to note that in the case of nonlinear spectral dispersion, a linear spectral phase of total range $512\pi$ across a 512-pixel LCM (an average of $\pi$ phase shift per pixel) is quite different from the case of a periodic $0\pi 0\pi\cdots$ phase modulation with average period one pixel. The former case is shown in Fig. 10 and gives one strong pulse and one weak one; the latter case is shown in Fig. 4 and gives two identical strong pulses.

## V. Conclusion

In summary, we have reported the first femtosecond pulse-shaping experiments using a 512-element liquid crystal phase-only modulator. Our results show that the increased pixel amount allows substantially enhanced pulse-shaping resolution and a greater temporal window (for fixed optical bandwidth) compared to the 128-element LCMs commonly available.

We have also performed preliminary adaptive pulse-shaping experiments, in which we have demonstrated that new patterns may be applied to the LCM every 90 ms, which is significantly faster than most current LCM drive electronics. This should translate into faster convergence in adaptive pulse-shaping routines. Finally, we have studied several effects that graphically illustrate the importance of accounting for the nonlinear spectral dispersion. We also show that the nonlinear spectral dispersion can substantially reduce the intensity of the replica pulses arising from the pixellated structure of liquid-crystal modulator pulse shapers.

## REFERENCES


[1] A. M. Weiner, "Femtosecond optical pulse shaping and processing," *Prog. Quantum Electron.*, vol. 19, pp. 161–238, 1995.

[2] ——, "Femtosecond pulse shaping using spatial light modulators," *Rev. Sci. Instrum.*, vol. 71, pp. 1929–1960, 2000.

[3] A. M. Weiner, D. E. Leaird, J. S. Patel, and J. R. Wullert, "Programmable shaping of femtosecond optical pulses by use of 128-element liquid-crystal phase modulator," *IEEE J. Quantum Electron.*, vol. 28, pp. 908–920, 1992.

[4] M. M. Wefers and K. A. Nelson, "Generation of high-fidelity programmable ultrafast optical wave-forms," *Opt. Lett.*, vol. 20, pp. 1047–1049, 1995.

[5] M. A. Dugan, J. X. Tull, and W. S. Warren, "High-resolution acousto-optic shaping of unamplified and amplified femtosecond laser pulses," *J. Opt. Soc. Amer. B*, vol. 14, pp. 2348–2358, 1997.

[6] P. J. Delfyett, L. T. Florez, N. Stoffel, T. Gmitter, N. C. Andreadakis, Y. Silberberg, J. Heritage, and G. Alphonse, "High-power ultrafast laser-diodes," *IEEE J. Quantum Electron.*, vol. 28, pp. 2203–2219, 1992.

[7] E. Zeek, K. Maginnis, S. Backus, U. Russek, M. Murnane, G. Mourou, H. Kapteyn, and G. Vdovin, "Pulse compression by use of deformable mirrors," *Opt. Lett.*, vol. 24, pp. 493–495, 1999.

[8] R. Bartels, S. Backus, E. Zeek, L. Misoguti, G. Vdovin, I. P. Christov, M. M. Murnane, and H. C. Kapteyn, "Shaped-pulse optimization of coherent emission of high-harmonic soft X-rays," *Nature* , pp. 164–166, 2000.

[9] A. Efimov, C. Schaffer, and D. H. Reitz, "Programmable shaping of ultrabroad-bandwidth pulses from a Ti-Sapphire laser," *J. Opt. Soc. Amer. B*, vol. 12, pp. 1968–1980, 1995.

[10] D. Yelin, D. Meshulach, and Y. Silberberg, "Adaptive femtosecond pulse compression," *Opt. Lett.*, vol. 22, pp. 1793–1795, 1997.

[11] L. Xu, L. Li, N. Nakagawa, R. Morita, and M. Yamashita, "Application of a spatial light modulator for programmable optical pulse compression to the sub-6-fs regime," *IEEE Photonic Technol. Lett.*, vol. 12, no. 11, pp. 1540–1542, 2000.

[12] H. Wang, Z. Zheng, D. E. Leaird, L. J. Friedman, and A. M. Weiner, "20-fs pulse shaping with a 512-element phase only liquid crystal modulator," in *12th International Conf. on Ultrafast Phenomena 2000*, Charleston, SC.

[13] P. F. McManamon, T. A. Dorschner, D. L. Corkum, L. J. Friedman, D. S. Hobbs, M. Holz, S. Liberman, H. Q. Nguyen, D. P. Resler, R. C. Sharp, and E. A. Watson, "Optical phased array technology," *Proc. IEEE*, vol. 84, no. 2, pp. 268–298, 1996.

[14] L. Wang and A. M. Weiner, "Programmable spectral phase coding of an amplified spontaneous emission light source," *Opt. Commun.*, vol. 167, pp. 211–224, 1999.

[15] S. T. Wu, "Birefringence dispersions of liquid-crystals," *Phys. Rev. A*, vol. 30, pp. 1270–1274, 1986.

[16] J. G. Proakis, *Digital Communications*, 3rd ed. New York: McGraw-Hill, 1995, pp. 724–726.

[17] A. M. Weiner and D. E. Leaird, "Generation of terahertz-rate trains of femtosecond pulses by phase-only filtering," *Opt. Lett.*, vol. 15, pp. 51–53, 1990.

[18] R. N. Thurston, J. P. Heritage, A. M. Weiner, and W. J. Tomlinson, "Analysis of picosecond pulse shape synthesis by spectral masking in a grating pulse compressor," *IEEE J. Quantum Electron.*, vol. 22, pp. 682–696, 1986.

**H. Wang** (S'96) was born in Wuhan, China, in 1975. He received the B.S. degree in electronic engineering from Tsinghua University, Beijing, China, in 1998. He is currently pursuing the Ph.D. degree in electrical and computer engineering at Purdue University, West Lafayette, IN.

Part of his work with optical pulse shapers was presented at the 12th International Conference on Ultrafast Phenomena 2000, Charleston, SC, and CLEO2001, Baltimore, MD. His main areas of research include optical pulse shaping and second harmonic generation.

**Z. Zheng** (S'97–M'00) was born in Beijing, China. He received the B. Eng. degree in electronic engineering from Tsinghua University, Beijing, China, in 1995, and the M.S.E.E. and Ph.D. degrees in electrical engineering from Purdue University, West Lafayette, IN, in 1997 and 2000, respectively.

In January 2001, he joined Lucent Technologies, Holmdel, NJ, as a Member of Technical Staff, where he is involved in the research and development of advanced optical-layer networking technologies and high-speed wavelength-division multiplexing systems. His research interests include high-speed lightwave communications, optical networking, nonlinear optics, and ultrafast optics.

Dr. Zheng is a member of IEEE/LEOS and the Optical Society of America (OSA).

**D. E. Leaird** (M'01) was born in Muncie, IN, in 1964. He received the B.S. degree in physics from Ball State University, Muncie, IN, in 1987, and the M.S. and Ph.D. degrees from the School of Electrical and Computer Engineering, Purdue University, West Lafayette, IN, in 1996 and 2000 respectively.

He joined Bell Communications Research (Bellcore), Red Bank, NJ, as a Senior Staff Technologist in 1987, and later advanced to Member of Technical Staff. From 1987 to 1994, he worked in the Ultrafast Optics and Optical Signal Processing Research Group, where he was a key team member in research projects in ultrafast optics, such as shaping of short optical pulses using liquid crystal modulator arrays, investigation of dark soliton propagation in optical fibers, impulsive stimulated Raman scattering in molecular crystals, and all-optical switching. He is currently a Research Engineer and Laboratory Manager of the Ultrafast Optics and Optical Fiber Communications Laboratory in the School of Electrical and Computer Engineering, Purdue University, where he has been since 1994. He has co-authored approximately 40 journal articles and 55 conference proceedings. His first U.S. patent is currently pending. Dr. Leaird has received several awards for his work in the ultrafast optics field including a Bellcore "Award of Excellence", a Magoon Award for outstanding teaching, and an Optical Society of America/New Focus Student Award.

**A. M. Weiner** (S'84–M'84–SM'91–F'95) was born in Boston, MA, in 1958. He received the Sc.D. degree in electrical engineering from the Massachusetts Institute of Technology (MIT), Cambridge, in 1984.

From 1979 through 1984, he was a Fannie and John Hertz Foundation Graduate Fellow at MIT. His doctoral thesis dealt with femtosecond pulse compression (including generation of the shortest optical pulses reported up to that time) and measurement of femtosecond dephasing in condensed matter. In 1984, he joined Bellcore, where he conducted research on ultrafast optics, including shaping of ultrashort pulses, nonlinear optics and switching in fibers, and spectral holography. In 1989, he became Manager of the Ultrafast Optics and Optical Signal Processing Research District. He joined Purdue University as a Professor of electrical and computer engineering in 1992. Since 1996, he has also been Director of Graduate Admissions for the School of Electrical and Computer Engineering. He spent the 1999–2000 academic year as a Visiting Professor at the Max Born Institute for Nonlinear Optics and Short Pulse Spectroscopy in Berlin, Germany. His current research interests center on processing of ultrashort pulses, high-speed optical communications, applications of pulse shaping to femtosecond spectroscopy and nonlinear optics, terahertz radiation, and optical imaging in scattering media. He has published four book chapters and approximately 100 journal articles. He is author or coauthor of 200 conference papers, including approximately 60 conference invited talks, and has presented more than 50 additional invited seminars at universities or industry. He has received five U.S. patents. He has served on or chaired numerous research review panels, professional society award committees, and conference program committees. He was General Co-Chair of the 1998 Conference on Lasers and Electro-optics and Chair of the 1999 Gordon Conference on Nonlinear Optics and Lasers. He was Associate Editor of *Optics Letters*.

Prof. Weiner is a Fellow of the Optical Society of America. He received the 1984 Hertz Foundation Doctoral Thesis Prize. In 1988–1989, he was selected as an IEEE Lasers and Electro-optics Society (LEOS) Traveling Lecturer. In addition, he was Associate Editor for the IEEE JOURNAL OF QUANTUM ELECTRONICS and IEEE PHOTONICS TECHNOLOGY LETTERS. He received the 1990 Adolph Lomb Medal from the Optical Society of America for pioneering contributions to the field of optics made before the age of 30. He received the Curtis McGraw Research Award of the American Society of Engineering Education (1997), the International Commission on Optics Prize (1997), the IEEE LEOS William Streifer Scientific Achievement Award (1999), and the Alexander von Humboldt Foundation Research Award for Senior U.S. Scientists (2000). He was an elected Member of the Board of Governors of the IEEE Lasers and Electro-optics Society from 1997 to 1999 and is currently Secretary/Treasurer of that organization.

**T. A. Dorschner** (S'68–A'73) received the B.S. degree in electrical engineering from the Massachusetts Institute of Technology, Cambridge, MA in 1965, and the M.S. and Ph.D. degrees in electrical engineering from the University of Wisconsin, Madison, WI, in 1967 and 1971 respectively.

From 1971 to 1973, he was a Research Associate in the Institut fr Hochfrequenztechnik at the Universitt Brauschweig, Braunschweig, Germany, where he worked in the microwave and quasi-optical communications fields, extending the theory of multiple-state modulators, and developing a gigahertz semiconductor modulator for an experimental millimeter-wave communication system. He joined the Research Division of the Raytheon Company in 1974, where he invented and helped to develop a nonplanar laser gyroscope. In 1984, he was named Manager of the Electro-Optics Laboratory of the Research Division, in which he has overseen work on gaseous and solid-state lasers, nonlinear optical devices, isolators and modulators, integrated optics, and most recently, optical phased arrays. He holds 20 US patents, has authored 17 scientific papers, and co-authored one book chapter.

Dr. Dorschner is a member of the Optical Society of America.

**J. J. Fijol**, photograph and biography not available at the time of publication.

**L. J. Friedman** (M'92) received the Ph.D. degree in experimental physics from Cornell University, Ithaca, NY.

From 1986 to 1989, he served on the research faculty in the University of Southern California physics department. While at USC his research was in the field of low-temperature physics. He joined the electro-optics group at Raytheon Research Division in 1989, working primarily on imaging diagnostics and numerical modeling in support of the development of optical phased arrays.

**H. Q. Nguyen** received the B.S. degree in electrical engineering from Wentworth Institute of Technology, Boston, MA, in 1988 and the M.S. degree in physics from the University of Massacusetts, Boston, MA, in 1992.

He joined Raytheon in 1988, where his work included laser deposition of YBCO superconducting thin films and development of phosphors for field emission displays. His most recent work has involved process development for the fabrication of optical phased arrays.

**L. A. Palmaccio**, photograph and biography not available at the time of publication.